Phys. Status Solidi B **249**, No. 2, 343–359 (2012) / **DOI** 10.1002/pssb.201100457

physica status solidi b
www.pss-b.com
basic solid state physics

Feature Article

In-Si(111)(4 × 1)/(8 × 2) nanowires: Electron transport, entropy, and metal-insulator transition

W. G. Schmidt*[,1], S. Wippermann[2], S. Sanna[1], M. Babilon[1], N. J. Vollmers[1], and U. Gerstmann[1]

[1] Lehrstuhl für Theoretische Physik, Universität Paderborn, 33095 Paderborn, Germany
[2] Department of Chemistry, University of California, One Shields Avenue, Davis, CA 95616, USA

Received 20 July 2011, revised 16 September 2011, accepted 26 September 2011
Published online 28 December 2011

Dedicated to Thomas Frauenheim on the occasion of his 60th birthday

Keywords charge-density wave, electron transport, entropy, in adsorption, nanowire, Peierls transition, Si(111) surface

* Corresponding author: e-mail w.g.schmidt@upb.de, Phone: +49-5251-602335, Fax: +49-5251-603435

In this paper the recent experimental and theoretical progress in understanding the properties of the In-Si(111)(4 × 1)/(8 × 2) nanowire array – a prototypical model system for exploring electron transport at the atomic scale – is reviewed. Density functional theory (DFT) calculations illustrate how strongly structural, vibrational, and electronic properties of atomic-scale wires are intertwined. Numerical simulations of the nanowire optical response in comparison with recent measurements settle eventually the long-standing debate on the nanowire ground-state geometry in favor of hexagons. Soft phonon modes are found to transform the nanowire structurally between the insulating hexagon structure and metallic In zigzag chains. The subtle balance between the lower energy of the insulating phase and the larger vibrational entropy of the metallic wires is demonstrated to cause the temperature-dependent phase transition. The dynamic fluctuation model proposed earlier to explain the phase transition is shown to contradict the experimental information on the metal insulator transition of the nanowires. The influence of adatoms on the quantum transport and phase transition is discussed.

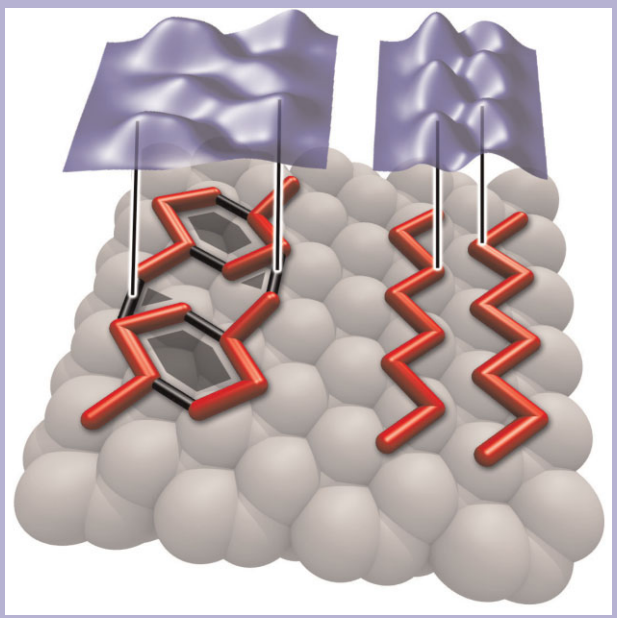

Schematic drawing of the main structural motifs of the In-induced Si(111)(8 × 2) and (4 × 1) reconstructions, In hexagons and zigzag chains, respectively.

1 Introduction One-dimensional (1D) electronic systems are expected to show interesting electronic features, such as spin-charge separation in a Luttinger liquid or Peierls instabilities [1, 2]. Atomic scale, quasi-1D, nanowires do also find increasing interest in the technological context of downsizing the microelectronics into the nanoscale regime. Highly anisotropic surface superstructures provide a interesting testbed to study both experimentally as well as computationally the interplay of structural, vibrational, and electronic properties of atomic-scale nanowires.

The ordered array of In ''nanowires'' formed upon room temperature (RT) In monolayer (ML) deposition and

subsequent annealing – probably first described by Lander and Morrison [3] – is arguably the most intensively investigated system of this kind. By now, experiment and theory have established a structural model (see top of Fig. 1) that is well accepted for the RT phase of the nanowire array [4–12]: each nanowire consists of two zigzag chains of In atoms within a (4 × 1) surface periodicity. The nanowires are separated by Si chains resembling the π-bonded chains of the clean Si(111)(2 × 1) surface.

In contrast to the RT structure and electronic properties of the clean In-Si(111)(4 × 1) surface that are meanwhile well understood, there are open questions concerning (i) the impact of the adsorption of foreign as well as In adatoms [13–15] on the In nanowire array and its properties, (ii) the geometry of the (8 × 2) reconstructed surface ground-state formed at low temperatures (LTs) [16, 17], and (iii) the driving force and mechanism of the temperature-induced (4 × 1) → (8 × 2) phase transition [18–21].

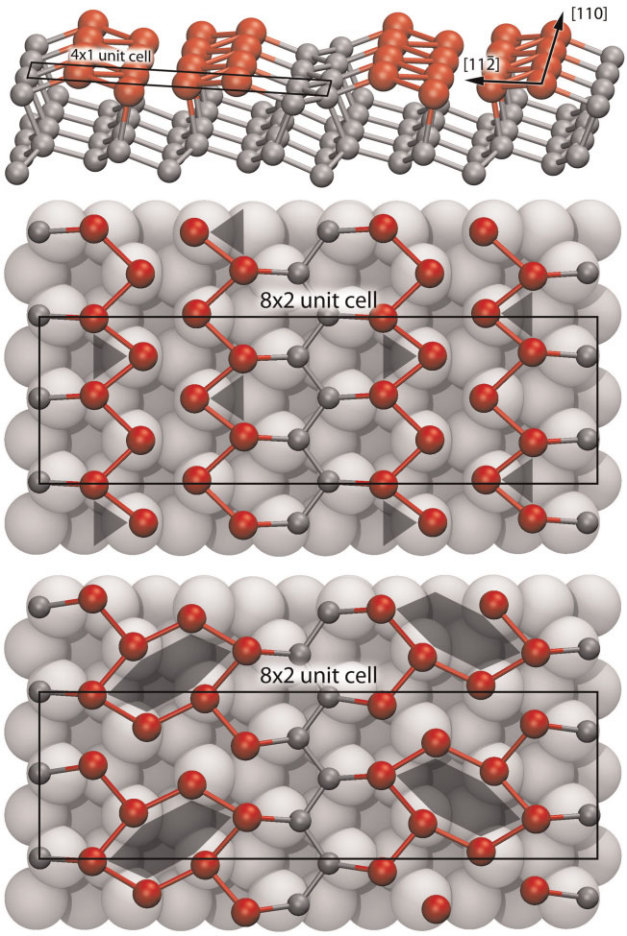

Figure 1 (online color at: www.pss-b.com) Perspective view of the In-Si(111)(4 × 1) nanowire array (top) as well as top views of two structural models discussed for the In-Si(111)(8 × 2) surface, trimer (middle) and hexagon model (bottom), respectively. Dark (red) and gray spheres indicate In and Si atoms, respectively.

In this paper the recent progress in clarifying these questions is discussed. Thereby, *first-principles* calculations are used to explain and rationalize experimental and theoretical findings.

2 Methodology Stekolnikov et al. [21] have carefully checked the influence of physical approximations within density functional theory (DFT) on the energetic and structural properties of the In-Si(111)(4 × 1)/(8 × 2) surface. They found a large influence of the d-electron treatment (core or valence) and the approximation for the electron exchange and correlation [local density approximation (LDA) *vs.* general gradient approximation (GGA)] on the ground state geometry. While a satisfactory explanation for this sensitivity (apart from the complexity of the surface structure and the small energy differences between competing structures) cannot be given in the moment, it may partially be related to the description of the In–In bonds. The peculiar low-symmetry ground state of bulk In is related to subtle electronic effects and – due to its low stabilization energy of only 2 meV per atom – is easily distorted [22]. The correct simulation of the pressure-induced phase transition of bulk In requires the inclusion of the relativistic mass velocity and Darwin terms as well as the treatment of the In 4d states as valence electrons [23]. Since the inclusion of relativistic effects is still out of reach for surface structures as large as considered here, we use a pragmatic approach in the present work: the comparison between calculated and measured fingerprints for the In-Si(111)(8 × 2) surface [21, 24] as well as the calculated transition temperature for the (4 × 1) → (8 × 2) phase change [25] suggests that LDA calculations where the In 4d electrons are frozen into the core describe the experiment well. This is the methodology used in the present work. In detail, we use DFT within the LDA [26] as implemented in VASP [27].

The In-Si(111) surfaces are simulated by repeated symmetric slabs with 12 Si bilayers and a vacuum region equivalent in length. The *k*-space integrations are performed using uniform meshes equivalent to 128 points in the (1 × 1) surface Brillouin zone for electronic structure calculations. The *k*-point density was increased for optical response and electronic-entropy calculations, where we used 960 points. The electron-ion interaction is described by projector-augmented wave (PAW) potentials. An energy cutoff of 250 eV was found to be sufficient to obtain converged results and has been used throughout the work.

The Landauer conductance in the limit of zero bias

$$G = \frac{2e^2}{h} M(E_F) T(E_F) \tag{1}$$

is calculated from the energy dependent number of modes M and transmission probability T using the WanT approach [28], *i.e.*, a Green function formalism based on "maximally localized Wannier functions" [29] as a minimal basis set. Thereby we exploit the fact that the In-related surface states close to the Fermi energy (E_F) depend very little on the

substrate [30] and study model structures that contain only the In and nearest neighbor Si atoms with the remaining Si dangling bonds terminated with hydrogen. Test calculations for structures with one and two Si bilayers [31] confirm the validity of this approach.

Reflectance anisotropy spectroscopy (RAS) is a powerful technique for probing optically anisotropic surface and interface structure [32]. It measures the difference in reflectance, at near normal incidence, of light linearly polarized in two orthogonal directions at the surface plane. The response depends on the imaginary part of the difference in the surface dielectric function in the two orthogonal directions. The reflection anisotropy $\Delta R/R$ for light polarized along α and β can be derived from slab calculations and is given by (see, *e.g.*, Refs. [33, 34])

$$\frac{\Delta R}{R} := \frac{R_\alpha - R_\beta}{R} = \frac{4\omega d}{c}\,\mathrm{Im}\left[\frac{4\pi\left[\alpha_{\alpha\alpha}(\omega) - \alpha_{\beta\beta}(\omega)\right]}{\varepsilon_\mathrm{b}(\omega) - 1}\right], \tag{2}$$

where $\varepsilon_\mathrm{b}(\omega)$ is the bulk dielectric function, and $\alpha_{\alpha\alpha}$ and $\alpha_{\beta\beta}$ are components of the optical polarizability tensor of the slab with thickness d. In the following, α and β are identified with the [110] and $[11\bar{2}]$ directions, respectively. In the present work the slab polarizability is calculated in the independent-particle approximation based on the electronic structure obtained within DFT-LDA. A scissors operator is used to correct the band-gap underestimation. Thereby a constant shift of 0.5 eV is applied to all unoccupied DFT eigenvalues that lie more than 0.5 eV above the highest occupied electronic state. This ensures an approximate reproduction of the measured Si bulk band structure. For the energetically lower lying unoccupied states a linear interpolation up to a zero shift for states directly at the Fermi energy is used in order to model the energy dependence of the electronic self-energy. Beyond this crude approximation of the self-energy, many-body effects such as excitonic and local-field effects [35, 36] are completely neglected. While this certainly results in a loss of quantitative accuracy and may affect the calculated line shape, past experience indicates that the calculated spectra can still be expected to be qualitatively reliable (see, *e.g.*, Ref. [34]). This holds in particular if differences and trends for very similar systems are considered, as in the present case.

3 Electron transport along the In-Si(111)(4 × 1) zigzag chains Crystal surfaces with atomically controlled structures are a very promising playground for studying low-dimensional transport phenomena, with expectations of advancing from mesoscopic to nanoscale transport physics. The In nanowire array formed by the In-Si(111)(4 × 1) surface lends itself to unambiguous, direct, and quantitative measurements of electronic transport through single-atomic layers: the nanowires are of high structural quality and can be reproducibly and relatively easily prepared. Moreover, the metallic In bands are effectively decoupled from the continuum of Si bulk states. Experimentally, a strongly anisotropic electrical conductance was measured, where the electron transport occurs preferentially along the In zigzag chains [37]. In fact, the surface-state conductance along the metallic atom chains $\sigma_{||}$ was found to be about 60 times larger than that in the perpendicular direction $\sigma_\perp$.

The electron transport is influenced by electron phonon coupling, scattering at defects and other electrons which can be approximately accounted for by a finite effective relaxation time $\frac{1}{\tau} = \frac{1}{\tau_{\mathrm{el-ph}}} + \frac{1}{\tau_{\mathrm{el}}} + \frac{1}{\tau_{\mathrm{defects}}}$, whereas several band structure related contributions gives rise to the conductivity: (i) the surface-state bands in the topmost layers, (ii) bulk-state bands in a space-charge layer beneath the surface, and (iii) bulk states in the substrate material. Based on an analysis of measured angle resolved photoemission (ARPES) data it was stated in Ref. [37] that "$\sigma_{||}$ is determined by the surface-state band dispersion, while $\sigma_\perp$ is dominated by the space-charge layer". The bulk states are in any event not expected to contribute to the anisotropy of the surface conductivity.

Based on the calculated band structure of the In-Si(111)(4 × 1) surface we analyze the contribution of the surface bands to the electron transport properties of the clean In nanowire array. Thereby we follow at first a semiclassical approach. Within the Drude picture the conductance σ is related to the mean electron density n and mass m by

$$\sigma = e^2 \cdot \tau \cdot \frac{n}{m}. \tag{3}$$

Starting from a linearized Boltzmann equation in the case of weak scattering and upon comparison with the Drude formula, one obtains (see Ref. [38])

$$\sigma_{ij} = e^2 \cdot \tau \cdot \frac{n}{m^*_{ij}}, \tag{4}$$

where the effective mass tensor is given by

$$\frac{1}{m^*_{ij}} = \frac{1}{4\pi^3\hbar}\int_{\mathrm{FS}} v_i(\boldsymbol{k}) v_j(\boldsymbol{k}) \frac{\mathrm{d}S_{\boldsymbol{k}}}{|\boldsymbol{v}(\boldsymbol{k})|}, \tag{5}$$

with $\boldsymbol{v} = \nabla E(\boldsymbol{k})/\hbar$. For free-electron band structures it can be shown in a straightforward way that m^*_{ij} reduces to the usual effective mass as defined by the second derivative of the electronic bands $E(\boldsymbol{k})$ averaged over the Fermi surface (FS)

$$\frac{1}{m^*_{ij}} = \frac{1}{S_\mathrm{F}}\int_{\mathrm{FS}} \frac{1}{\hbar^2}\frac{\partial^2 E(\boldsymbol{k})}{\partial k_i \partial k_j}\mathrm{d}S_{\boldsymbol{k}}. \tag{6}$$

Here S_F is the area of the FS. In both formulas, the conductivity is, thus, determined by the band structure at the FS. In Fig. 2 the FS of the In-Si(111)(4 × 1) system is shown for the irreducible part of the surface Brillouin zone. The three bands contributing to the conductivity are analyzed according to Eqs. (5) and (6) using an $n \times 1 \times 1$ equidistant

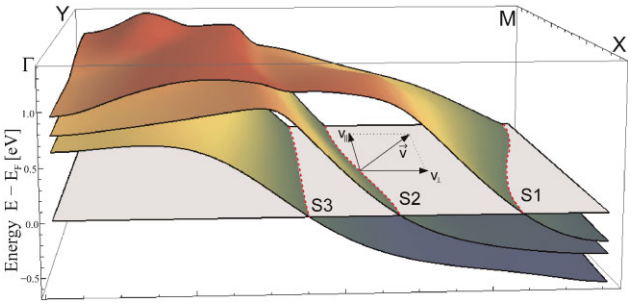

Figure 2 (online color at: www.pss-b.com) Dispersion of the In-related surface states of the In-Si(111)(4 × 1) nanowire array calculated from DFT-LDA for the irreducible part of the surface Brillouin zone.

k-point mesh along the FS. Note that for $T = 0$ K the FS reduces to a 1D line (see dashed line in Fig. 2). Equation (5) depends critically on the k-point sampling. Having in mind, that usually a limited data set is available from ARPES measurements this formula has to be used with great care if applied to experimental data.

In this sense, the formula 6 is more convenient to use. As shown in Table 1, the values for the effective mass tensor converge rapidly with increasing density of the k-point sampling. Thereby the contributions to $\sigma_{||}$ along the In zigzag chain are comparable for the three bands. In case of the $8 \times 1 \times 1$ sampling, the values for S_1 and S_3 are almost the same, S_2 is moderately larger by about 50%. The contributions to $\sigma_{\perp}$ perpendicular to the In chains are quite different for the three surface states. The contribution of S_3 is smaller by more than an order of magnitude, in agreement with its nearly vanishing dispersion along this direction (see Fig. 2). As a consequence, the three bands contribute in a different way to the anisotropy in surface conductivity.

Table 1 Elements of the effective mass tensor [m_e] estimated from an analysis of the FS using equidistant $n \times 1 \times 1$ k-point sets. Values split up into the contributions of the three bands S_1, S_2, S_3 are also given.

k-point mesh	band	$\left(\frac{1}{m^*}\right)_{\|\|}$	$\left(\frac{1}{m^*}\right)_{\perp}$	$\sigma_{\|\|}/\sigma_{\perp}$
	S_1	0.7800	0.0146	53.42
$2 \times 1 \times 1$	S_2	1.1300	0.0118	95.76
	S_3	0.6900	0.0008	862.50
	FS	0.8600	0.0091	93.92
	S_1	0.8974	0.0053	170.94
$4 \times 1 \times 1$	S_2	1.0722	0.0331	32.39
	S_3	0.7122	0.0022	323.72
	FS	0.8939	0.0135	66.05
	S_1	0.7762	0.0149	52.09
$8 \times 1 \times 1$	S_2	1.1580	0.0283	40.92
	S_3	0.7339	0.0018	407.72
	FS	0.8894	0.0150	59.29

Averaging over the three bands, however, we calculate a value $\sigma_{||}$ along the In-chain that exceeds the one in the perpendicular direction by a factor of 59, in very good agreement with the experimental ratio $\sigma_{||}/\sigma_{\perp}$ of about 60. It is noteworthy that the measured anisotropy of the surface conductivity could be reproduced solely on the basis of the dispersion of the surface states at the Fermi level. There is no need to assume – as done in Ref. [37] – a contribution from the space-charge layer beneath the surface.

Obviously, the experimental findings for the clean, (4×1) reconstructed nanowire array are well described by the present DFT calculations. Experimentally, the modification of the In nanowire structural and electronic properties upon adsorption of foreign as well as In adatoms [13–15] and the corresponding electron transport properties [39] have found much interest. It was found that the conductivity of the – at RT metallic [37, 40] – In nanowires is roughly halved by adsorbing additional In (0.1 ML) on top of the wires [39]. The mechanism that quenches the conductance, and the impact of other species on the wire resistance is not clear, however.

In order to address these issues the potential energy surfaces (PESs) for In, Pb, H, and O adsorbed on the nanowire array were determined in Ref. [41]. In all cases, clearly corrugated energy landscapes were obtained. In, O, and Pb prefer a position between neighboring In chains and H bonds to a surface silicon atom. While the lateral positions of In, O, and Pb adatoms are nearly equal, the adsorption geometry is not. The In and O adatoms are located almost in-plane with the In chain atoms, whereas Pb prefers a pyramidal configuration, see Fig. 3. This affects also the structural relaxation of the In nanowire. Comparatively small deformations occur for Pb, but larger atomic shifts are found for In and O deposition. This is reflected in the standard deviation of the In–In bond length distribution calculated for ideal and adatom-modified In nanowires, see Table 2.

Starting from the relaxed adatom positions, the influence of the perturbation on the In nanowire conductance is calculated. Obviously, a treatment on a quasi-classical level as successfully applied to the clean surface will not suffice

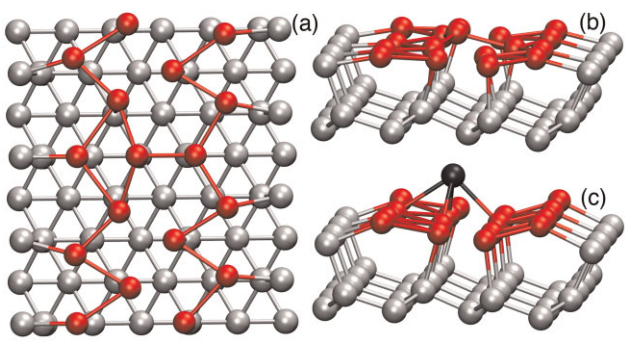

Figure 3 (online color at: www.pss-b.com) Top (a) and side view (b) of In adatoms adsorbed on the In/Si(111)(4 × 1) surface. The side view of the Pb adatom is shown in (c).

Table 2 Standard deviation σ_s of the In–In bond length distribution for ideal and defect-modified nanowires. Average quantum conductance G in the energy interval ± 0.05 eV around E_F, G' refers to the respective adatom structure without the adatom. The last column contains the electronic DOS at E_F.

adatom	σ_s (Å)	$G\left(\frac{2e^2}{h}\right)$	$G'\left(\frac{2e^2}{h}\right)$	DOS (a.u.)
ideal	0.01	3.75	3.75	0.70
In	0.12	2.31	2.77	0.95
Pb	0.07	3.11	3.72	1.23
H	0.04	3.60	3.74	1.44
O	0.11	2.43	3.25	1.22

anymore. We follow the Landauer approach and use in the following a lead-conductor-lead partitioning of the system. Here, the In chain segment with the adatom forms the conductor and the semi-infinite leads are modeled with ideal In nanowires. The calculated conductance spectra of the ideal and adatom perturbed In nanowires are shown in Fig. 4. For In adatoms, a reduction of the quantum conductance at E_F by more than one third compared to the ideal chain is calculated. While the experimental conditions are not sufficiently well defined to allow for a quantitative comparison with the available measurements, the calculated reduction is of the same order as measured [39]. Interestingly, apart from hydrogen which does not substantially modify the electron transport properties, the calculations predict distinct conductance drops as well for Pb and in particular for O, see Table 2. Naively, one might want to explain this finding with a reduced density of electronic states [density of states (DOS)] at E_F. However, as shown in Fig. 4 and Table 2, (i) the DOS increases irrespective of the specific adatom deposited and (ii) the increase of the DOS shows no clear correlation with the modification of the conductance. For example, the DOS at E_F is larger for Pb and O than for In adatoms. However, In is most effective in reducing the conductance. Obviously, the total DOS allows no quantitative predictions about the conductance.

This holds also for the local density of states (LDOS). The adsorption of Pb leads to a very localized LDOS modification – illustrated in Fig. 5 – whereas the adsorption of In adatoms modifies the LDOS even more than 10 Å away from the adsorption site (not shown here). In all cases apart from oxygen, where a small reduction occurs, the LDOS projected on the wire direction increases at the adatom position. Its modification shows no clear trend with the change of the nanowire conductance.

In the case of CO adsorption on substrate-supported Au chains, the drastic conductance drop could be traced to an electron localization effect, induced by the deep potential well arising at the adsorption site [42]. In order to see if a similar mechanism acts here, the local effective potential has been extracted from the DFT calculations. This potential is then averaged in a plane perpendicular to the nanowire direction chosen large enough to contain – within their covalent radii – the nanowire In atoms as well as the adatoms. As shown in Fig. 6, the systems studied here differ drastically

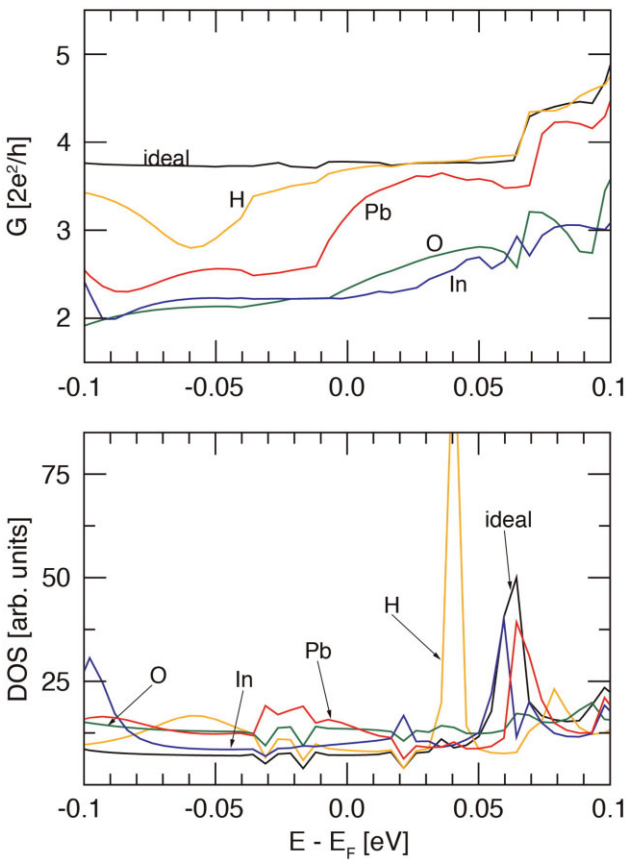

Figure 4 (online color at: www.pss-b.com) Quantum conductance spectrum for electron transport along the wire direction (upper part) and total DOS (lower part) calculated for ideal and adatom-modified In/Si(111) structures.

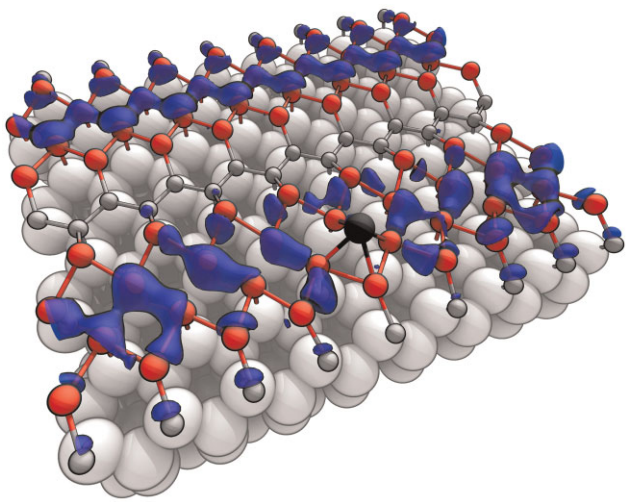

Figure 5 (online color at: www.pss-b.com) Isodensity surface of the LDOS at E_F, illustrating the LDOS at the ideal In nanowires and its modification upon Pb adsorption.

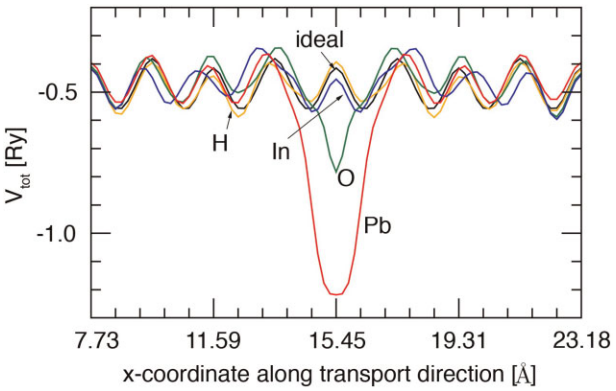

Figure 6 (online color at: www.pss-b.com) Averaged (see text) effective potential along the wire direction calculated for ideal and adatom-modified In/Si(111) structures.

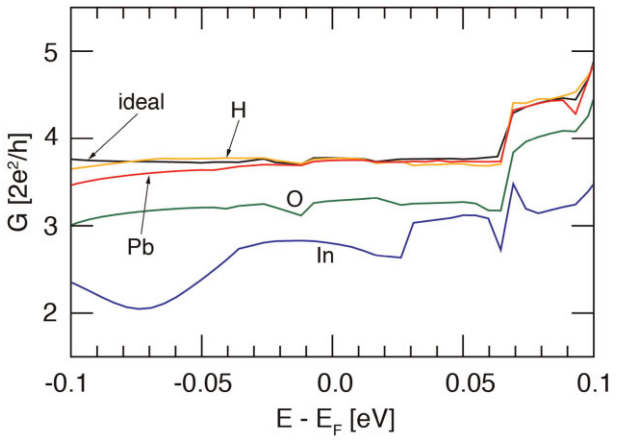

Figure 7 (online color at: www.pss-b.com) Quantum conductance spectrum for electron transport along the wire direction calculated for ideal and adatom-modified In/Si(111) structures that do, however, not contain the adatom.

with respect to the local potential. A very deep potential well is formed upon Pb adsorption, while additional In atoms barely change the potential along the wire direction. Thus, it seems likely that the conductance modification upon Pb adsorption obeys a similar mechanism as proposed for CO adsorbed on Au chains [42]. Judging from Fig. 6, however, this mechanism cannot explain the conductance drop upon In deposition: In adatoms drastically reduce the In nanowire transmittance without giving rise to large potential fluctuations. These considerations are corroborated by 1D model calculations, where the time-dependent Schrödinger equation for the potentials shown in Fig. 5 is solved. The transmission of Fermi wave-vector electrons across the Pb potential well is reduced by 8%, while we obtain a reduction by only 3% in case of In.

In order to understand the conductance drop in the latter case, it is helpful to come back to the initial observation that the adatoms deform the nanowire to different degrees. While the smallest deformations are observed for H and Pb adsorption, In causes large deformations (*cf.* Table 2). The computational modeling allows for separating the impact of the adatom-induced structure deformation from the impact of the adatom itself: transport calculations were performed for nanowire structures that are deformed according to their relaxation in response to the adatom, but do *not* contain the adatom. The results are shown in Fig. 7 and compiled in Table 2. As can be seen here, the – comparatively small – geometry changes of the In nanowire upon adsorption of hydrogen or lead do not substantially reduce the wire conductance. This is in contrast to the stronger deformations caused by the adsorption of oxygen or indium, where moderate to strong conductance reductions are calculated.

This does now allow for a classification of the adatom induced conductance modifications. Pb adsorption does not substantially modify the nanowire geometry, but forms a deep potential well that effectively scatters the electrons and thus reduces the transmittance. In the case of In no potential well is formed. Here, the conductance drop is related to the wire deformation. Both factors contribute in the case of oxygen. A moderate potential well is formed and on top of that the nanowire gets somewhat deformed. This results in a conductance drop of similar magnitude as calculated for In. Hydrogen, finally, does neither act as a potential well nor does it deform significantly the nanowire. Consequently, it has no substantial impact on the electron transport.

4 Low-temperature In-Si(111)(8 × 2) geometry

Yeom et al. [16] reported that In-Si(111)(4 × 1) undergoes a reversible phase transition below 120 K to an (8 × 2) structure, with a strong reduction of the DOS at the Fermi energy. From photoemission and scanning tunneling microscopy (STM) studies they concluded that this phase formed a 1D charge-density wave (CDW) system driven by a Peierls instability. These intriguing results provoked much experimental and theoretical work. However, the mechanism of the (4 × 1) → (8 × 2) phase transition as well as the LT ground-state and its properties remain controversial. While the RT (4 × 1) phase is a quasi-1D metal as shown above, it has been variously suggested that the LT (8 × 2) phase is metallic, but with a lower DOS at the Fermi level [19, 43, 44], semimetallic [19], and semiconducting with a fundamental energy gap of 0.1–0.3 eV [16, 39, 45–47]. Most *ab initio* calculations predict the nanowire ground state to be characterized by the formation of In trimers (*cf.* middle panel in Fig. 1) and find no gap opening [5, 8, 10, 12]. However, also an In hexagon structure resulting from shear distortions in neighboring chains (*cf.* bottom panel in Fig. 1), has been predicted, which is semiconducting [20]. Total-energy calculations [21] of the hexagon and the trimer model for the LT phase concluded that an unambiguous identification of the internal structure of the ground state on energetic arguments is problematic. The energy differences between the competing structures are very small and depend on the approximations made in

the calculations, *e.g.*, the treatment of the In 4d states, and exchange and correlation effects. Cho and Lee [48] state that the hexagon model is not stable, but the model has been supported recently by positron diffraction studies [49].

Given the ambiguities of the total-energy calculations in determining the ground-state structure of the (8×2) phase, the comparison of fingerprints calculated for structural candidates with measured data may be helpful. The calculated optical anisotropies [8] for the (4×1) and the trimer-reconstructed (8×2) nanowire arrays are compatible with the measured evolution of the surface optical response during the $(4 \times 1) \rightarrow (8 \times 2)$ phase transition [9]: RAS data measured for the In-Si(111)(4×1) surface [50–52] show an optical anisotropy in the energy region of 2 eV, which splits into two peaks, at 1.9 and 2.2 eV, upon formation of the LT phase of the In-Si(111) surface [9, 53]. Wippermann and Schmidt [54] have shown that also the hexagon model provides an optical signature that describes the experimental findings for the LT phase equally well as the trimer model, at least within the energy window considered in Refs. [50–52], *i.e.*, for photon energies above about 1 eV. On the other hand, the small differences in geometry of the trimer and hexagon model lead to significant changes in the band structure near the Fermi level [20, 21]. Optical transitions in this energy region are expected to be very sensitive to such changes. In fact, recent measurements of optical excitations in the mid-infrared (IR) spectral range from 0.31 to 0.99 eV show distinct differences in the optical response of the LT and RT phase of the In nanowire array [24]. Figure 8 shows the measured data. A smooth increase of the RAS signal is observed going to low energy for the RT (4×1) phase, while the LT (8×2) phase shows two sharp positive peaks at 0.50 and 0.72 eV. Positive anisotropy indicates that optical transitions parallel to the chains are dominant in this spectral region. Both phases show the broader, negative 1.9 eV feature, which splits below the phase transition temperature [8, 53, 54].

Also shown in Fig. 8 are the theoretical data from the DFT calculations. The calculated anisotropy of both the trimer and hexagon models of the (8×2) structure agree well with the experiment above 0.7 eV, as has been discussed in Ref. [54]. However, below 0.7 eV, only the hexagon model looks similar to the experimental results. In particular, two positive peaks are predicted, separated by 0.24 eV. This splitting agrees very well with the experimental splitting of 0.22 eV. The origin of the two peaks in the mid IR can be traced to optical transitions close to the M and X point of the surface Brillouin zone, as indicated by P_1 and P_2/P_2' in Fig. 9. Around these points, nearly parallel valence and conduction bands close to the Fermi level give rise to a high joint DOS. From the orbital character of states (shown in Fig. 10) we can assign P_1 to transitions between bonding and non-bonding In chain states within the single In zigzag chains, while P_2 and P_2' involve in addition In–In bonds between the two parallel zigzag chains. These bonds are exclusively formed for the hexagon model (bottom in Fig. 1). The spectra measured in the mid-IR are thus directly related to the hexagon structure of the In nanowire array. We mention, however, that the detailed analysis of the calculated RAS signal (*cf.* Ref. [55]) shows that additional contributions to the optical signal stem from inside the Brillouin zone.

Detailed comparison reveals that the calculated mid-IR peaks are redshifted by about 0.2 eV (note the different scales in Fig. 8). The underestimation of excitation energies is typical for DFT calculations where self-energy effects are neglected. The complexity and size of the In nanowire structure prevents the calculation of optical spectra using many-body perturbation theory that includes self-energy and excitonic effects [35]. Quasiparticle calculations for the high-symmetry points of the hexagon model surface band structure found self-energy effects to increase the lowest transition energies by 0.26 eV on average [21]. A larger

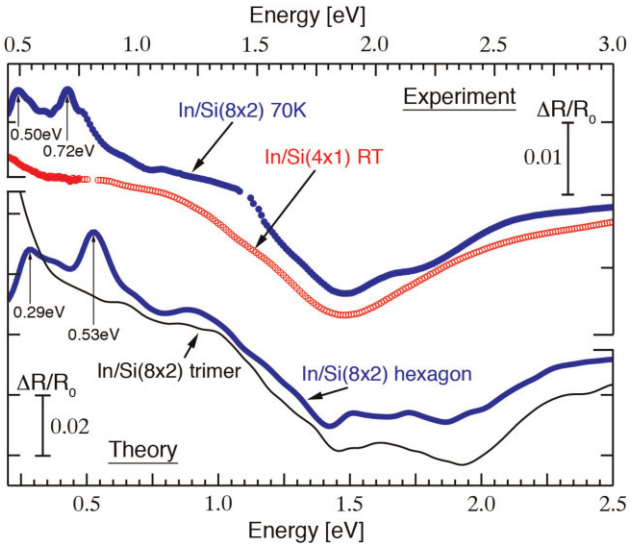

Figure 8 (online color at: www.pss-b.com) RAS spectra of In-Si(111)(4×1) at RT (300 K) and In-Si(111)(8×2) at LT (70 K): upper, experiment; lower, theory. Note the different scales.

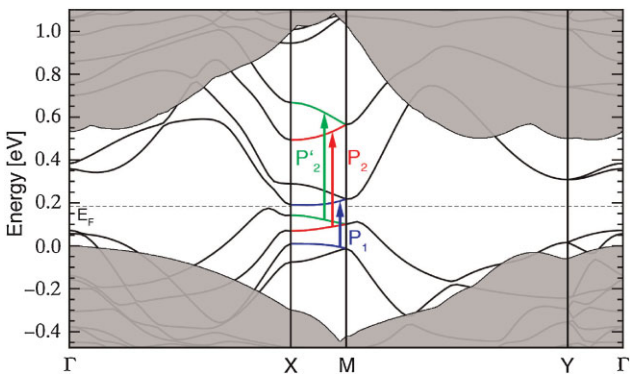

Figure 9 (online color at: www.pss-b.com) Band structure of the hexagon model for In-Si(111)(8×2). Pronounced optical transitions showing up in the RAS spectra are marked. Gray regions correspond to the projected Si bulk bands.

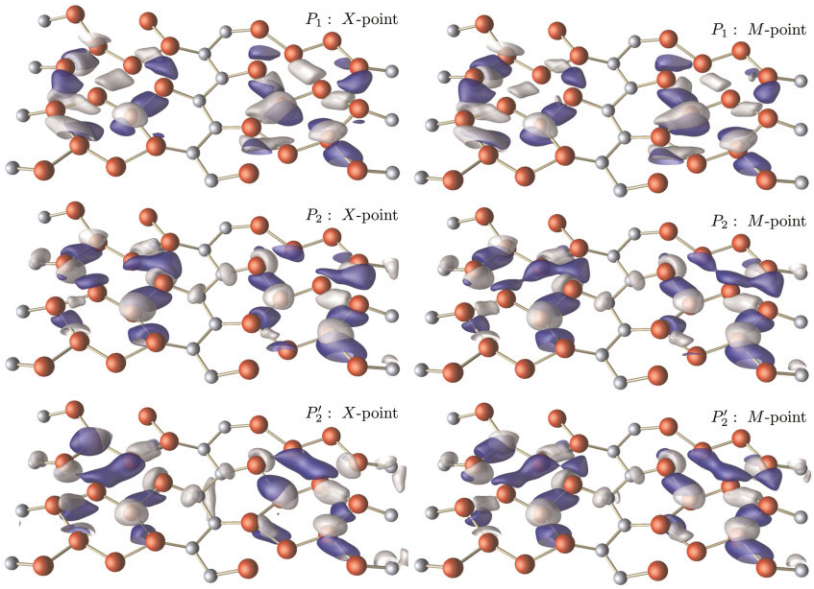

Figure 10 (online color at: www.pss-b.com) Orbital character of surface electronic states at the X and M high-symmetry points that contribute strongly to the optical anisotropy of the hexagon model for the In-Si(111)(8 × 2) nanowire array in the mid-IR regime. The notation is consistent with Figs. 8 and 9. The isosurfaces are drawn for a density of 0.0015 Å^3. Blue and white isosurfaces correspond to valence and conductance states, respectively.

shift of 0.5 eV, typical for Si excitation energies [35], applies to the higher energy negative optical anisotropies, because the optical transitions involve Si states [54]. Allowing for these energy shifts, the agreement between the calculated and measured RAS spectra is truly impressive and provides very strong evidence for the hexagon structure.

5 Metal–insulator transition What remains still an open question, however, is the nature and driving force of the metal-insulator transition. Originally, it was explained as a CDW formation due to the Peierls instability [16]. However, the phase transition cannot be based on a simple CDW model because only one of the metallic bands nests properly [19, 39, 45, 47, 56]. A triple-band Peierls instability has been proposed, where an interband charge transfer modifies the FS to improve nesting [30, 47, 57], while a periodic lattice distortion that lowers the energy has also been suggested [5, 10, 12, 43, 58]. On the other hand, many-body interactions were made responsible for the LT phase [13]. Several theoretical studies proposed the phase transition to be of order–disorder type [5, 20, 59] and explained the RT phase in terms of dynamic fluctuations between degenerate ground state structures. However, photoemission [46, 60] and Raman spectroscopy [61] results have cast doubt on this model.

In order to address this issue, free-energy calculations [25] were performed where in contrast to earlier work, the vibrational and electronic entropy of the In nanowire array is included in the calculations. For a fixed stoichiometry, the ground state of the surface-supported nanowires is characterized by the minimum of the free energy F as a function of the substrate crystal volume V and the temperature T. It can be obtained using atomistic thermodynamics, see, *e.g.*, Ref. [62]. Within the adiabatic approximation, F is given by

$$F(V,T) = F_{\rm el}(V,T) + F_{\rm vib}(V,T), \tag{7}$$

with $F_{\rm el} = E_{\rm tot} - TS_{\rm el}$, where the total energy $E_{\rm tot}$ is approximated by the zero-temperature DFT value and the electronic entropy $S_{\rm el}$ is obtained from

$$S_{\rm el} = k_{\rm B} \int {\rm d}E\, n_{\rm F}[f \ln f + (1-f) \ln (1-f)]. \tag{8}$$

Here $n_{\rm F}$ and f denote the density of electronic states and the Fermi distribution function, respectively. The vibrational free energy of the supercell with volume Ω is calculated in harmonic approximation

$$F_{\rm vib} = \frac{\Omega}{8\pi^3} \int {\rm d}^3\boldsymbol{k} \sum_i \left(\frac{1}{2}\hbar\omega_i(\boldsymbol{k}) + k_{\rm B}T \ln\left(1 - e^{-\frac{\hbar\omega_i(\boldsymbol{k})}{k_{\rm B}T}}\right)\right). \tag{9}$$

The wave-vector dependent phonon frequencies $\omega_i(\boldsymbol{k})$, as well as the corresponding eigenvectors are obtained from the force constant matrix calculated by assuming $F_{\rm el}(V,T) \sim E_{\rm tot}(T=0)$, *i.e.*, neglecting the explicit temperature and volume dependence. Given the extremely flat PES of the In-Si(111) system – that renders already the search for the minimum energy structure a difficult problem [5, 21, 48] – the uncertainties induced by the above approximations are expected to be small compared to the overall error bar of the calculations.

The calculated Γ-point frequencies for strongly surface-localized vibrational modes of the In-Si(111) nanowire array are compiled in Table 3. The table contains the present results for the (4 × 1) phase as well as their

Table 3 Calculated Γ-point frequencies for strongly surface localized A′ (upper part) and A″ phonon modes (lower part) of the In-Si(111)(4 × 1)/(8 × 2) phases. The symmetry assignment of the (8 × 2) modes is only approximate, due to the reduced surface symmetry.

present results ω_0 (cm^{-1})		
(4 × 1)	→	(8 × 2)
22	→	20
		27
		hexagon rotary mode
44	→	47
51	→	53
62	→	58, 69
65, 68	→	70, 69, 78, 82
100, 104	→	97, 106, 113, 142
129, 131	→	137, 142
143, 145	→	139, 145, 146, 147
28	→	18, 19
shear mode		
	→	antisym./sym. shear mode
		35
		51
		75
		82

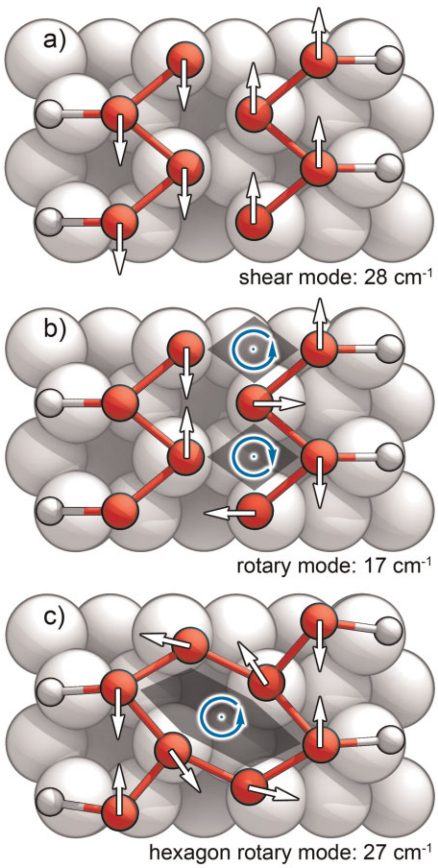

Figure 11 (online color at: www.pss-b.com) Calculated eigenvectors for three prominent phonons modes (notation as in Table 3) of the In-Si(111)(4 × 1) (a,b) and In-Si(111)(8 × 2) phase (c). The mode shown in (b) – occurring at the *X* point of the (4 × 1) BZ – is twofold degenerate due to the existence of an equivalent mode at the neighboring In chain.

assignment to the frequencies of geometrically similar eigenvectors of the (8 × 2) phase. The comparison with the Raman data from Fleischer et al. [61] shows that measured and calculated frequencies of the (8 × 2) phase agree typically within a few cm^{-1}, while the deviations between experiment and theory are slightly larger for the (4 × 1) modes. This indicates that anharmonicity effects neglected here affect the modes of the RT phase more noticeably than the LT data.

Interestingly, the calculations confirm the existence of a low-frequency shear mode of A″ symmetry for the In-Si(111)(4 × 1) phase at 28 cm^{-1}. This mode, which was also detected by Raman spectroscopy [61], is energetically below the phase transition temperature of about $k_B T \sim 83$ cm^{-1} and has been suggested to correspond to the lattice deformation characteristic for the (4 × 1) → (8 × 2) phase transition [20, 30, 59]. The calculated eigenvector of this mode (Fig. 11a) shows the two In atom zigzag chains oscillating against each other. This deviates somewhat from earlier predictions [63], but agrees with recent *first-principles* molecular dynamics (MD) simulations [20, 59]. In fact, the structural transformation from the In zigzag-chain structure with (4 × 1) symmetry to the In hexagons with (8 × 2) translational symmetry (Fig. 1) is perfectly described by superimposing the calculated eigenvector of the 28 cm^{-1} mode with the two degenerate low-frequency *X* point modes at 17 cm^{-1} (one of the symmetrically equivalent modes is shown in Fig. 11b). Similarly, the combination of the corresponding shear mode of the In-Si(111)(8 × 2) phase at 18 cm^{-1} with the hexagon rotary mode at 27 cm^{-1} (Fig. 11c) transforms the In hexagons back to parallel zigzag chains. The calculated phonon modes support the geometrical path for the phase transition proposed in Refs. [20, 30, 59]. In fact, they give an atomistic interpretation of the triple-band Peierls model [17, 30, 47]: the soft shear mode lifts one metallic band above the Fermi energy, while the rotary modes lead to a band-gap opening for the remaining two metallic In surface bands.

What, however, is causing the phase transition? In Fig. 12 we present the free energy difference between the In-Si(111)(4 × 1) and In-Si(111)(8 × 2) phases. It vanishes at 128.5 K if only the vibrational free energy is taken into account. Additional consideration of the electronic entropy lowers the calculated phase transition temperature to 125 K. At this temperature, the vibrational and electronic entropy is large enough to compensate for the lower total energy of the insulating (8 × 2) phase compared to the metallic (4 × 1) phase. The calculated phase transition temperature is slightly above the experimental value of about 120 K. Still, given the sensitivity of the total-energy calculations with respect to the approximations used for modeling the XC energy and the In 4d states discussed above,

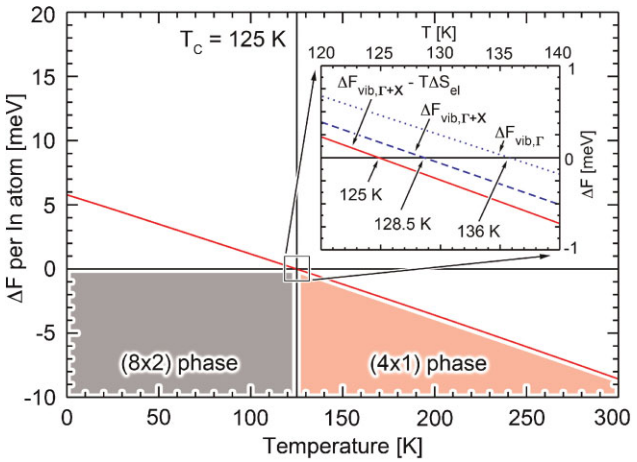

Figure 12 (online color at: www.pss-b.com) Difference of the free energy $F(T)$ calculated for the (4×1) and (8×2) phase of the In-Si(111) nanowire array. The stable phase is indicated. The inset shows enlarged the entropy difference calculated by neglecting the electronic contributions and by restricting the BZ sampling to the Γ point.

the agreement between theory and experiment should be considered to be fortuitously close.

The present calculations show that the phase transition is caused by the gain in (mainly vibrational) entropy that overcompensates for higher temperatures the gain in band-structure energy realized upon transforming the metallic In zigzag chains into semiconducting In hexagons. Indeed, a general trend to higher surface phonon frequencies upon hexagon formation is clearly observed. This can be seen from most values in Table 3 – with the shear mode as a notable exception – as well as from the comparison of the respective phonon densities of states shown in Fig. 13. The

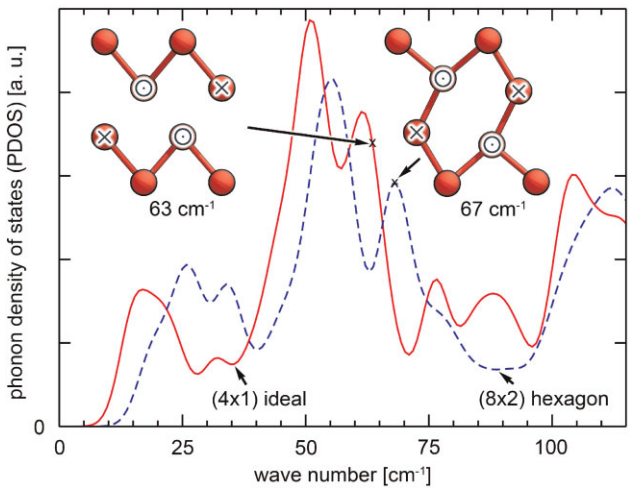

Figure 13 (online color at: www.pss-b.com) Phonon DOS calculated for the (4×1) and (8×2) phase of the In-Si(111) nanowire array ($4\,\mathrm{cm}^{-1}$ broadening). The inset shows a specific displacement pattern that hardly changes upon the phase transition but shifts in frequency. Arrows (feathers/heads) indicate down/up movements.

present calculations essentially confirm earlier experimental work that states "all major modes of the (4×1) surface are found in the (8×2) spectra, though blueshifted" [61]. A typical example is shown as inset in Fig. 13. The eigenvector corresponding to the alternating up and down movements of the In atoms hardly changes upon the (4×1)–(8×2) phase transition. The according frequency, however, goes up from 63 to 67 cm^{-1}. This shift in frequency is easily understood from the formation of additional In–In bonds upon hexagon formation, resulting in larger force constants.

The free energy calculations thus explain the (4×1)–(8×2) phase transition of the In-Si(111) nanowire array in terms of a subtle interplay between the lower total energy of the insulating In hexagon structure and the larger vibrational and electronic entropy of the less tightly bound and metallic In zigzag chain structure at finite temperatures. Accordingly, both the (4×1) and (8×2) phases are stable and well-defined structural phases [25]. This contradicts earlier DFT results where the (4×1) reconstruction is interpreted as time-averaged superposition of (8×2) units, *i.e.*, the dynamic fluctuation model [5, 20, 59]. In order to clarify the question whether or not two distinct and ordered phases exist, the calculated spectral signatures should be compared with the experimental findings. On the one hand, the overall good description of the distinct, but similar, sets of vibrational modes measured for the LT and RT phase by calculations for (8×2) and (4×1) geometries is a strong argument against the dynamical fluctuation model. Also, if at elevated temperatures the system were frequently visiting configurations associated with (8×2) structures, significant contributions from the LT structure should be present in the RT spectra, in contrast to the actual experimental findings [61].

The hypothesis of the dynamic fluctuation model rests essentially on *ab initio* MD calculations [20]. In order to assess the reliability of such calculations, we perform MD calculations and use the obtained snapshot structures as input for electron transport calculations. In detail, the temperature-dependent conductance is calculated by averaging over the individual conductances of random configurations obtained from either frozen phonon (FP) or MD calculations, respectively. After an equilibration time of 5000 steps with a time-step of 2 fs, 30 MD configurations have been selected randomly from MD runs at 50 and 300 K in each case. The required FP configurations are generated by relating the potential energy resulting from the elongation of the mode m to the expectation value of the energy according to

$$\sum_i \frac{1}{2} M_i \omega_m^2 \left(\frac{1}{\sqrt{M_i}} b_m(T) \boldsymbol{u}_{i,m} \right)^2 = \left(\overline{n}_m(T) \frac{1}{2} \right) \hbar \omega_m, \tag{10}$$

where M_i denotes the mass of atom i and ω_m, $\boldsymbol{u}_{i,m}$ are the modes eigenfrequency and eigenvector, respectively. The mode occupation is determined by the Bose–Einstein

distribution

$$\overline{n}_m(T) = \left[e^{\left(\frac{\hbar\omega_m}{k_B T}\right)} - 1 \right]^{-1}. \quad (11)$$

Solving this equation for the temperature-dependent scaling factor $b_m(T)$ yields the maximum elongation of the mode m at the temperature T. Subsequently, 30 configurations are generated by superimposing the modes with random phase factors for $T = 0$, 50, and 300 K, respectively. The non-zero temperature quantum conductance in linear response [generalization of Eq. (1)] is then be obtained from the band structures of the individual configurations according to

$$G = \frac{2e^2}{h} \int \mathrm{d}E\, \overline{T}(E) \left(-\frac{\partial f_0}{\partial E} \right), \quad (12)$$

where $\overline{T}(E)$ and f_0 denote the transmission function and Fermi distribution, respectively. Neglecting the contact resistances, $\overline{T}(E)$ is equal to the number of bands at energy E. To approximately account for self-energy effects, a constant shift of 0.5 eV is applied to all unoccupied DFT eigenvalues that lie more than 0.5 eV above the highest occupied electronic state, ensuring an approximate reproduction of the measured Si bulk band structure. For the energetically lower lying conductance states a linear interpolation up to a zero shift for states directly at the Fermi level models the energy-dependence of the electronic self-energy. This approach equals the one used for the optical response calculations in Section 4.

The number of bands at an energy E in the linear response expression Eq. (12) needs to be known with high accuracy. We find that using a dense k-point sampling alone does not necessarily lead to converged results if no information about the energy ordering of the eigenstates in the vicinity of a specific k point is available. Therefore, we project the wave functions on atomic orbitals centered at the positions of the ions and derive a k-point dependent numerical fingerprint of the orbital character of the respective electronic states. This fingerprint is then used to determine which electronic states adjacent in k space belong to the same band. The number of bands in interjacent k-space regions is then linearly interpolated.

The resulting averaged conductances obtained from both the FP and MD approaches are compiled in Table 4. At $T = 0$ K only zero-point vibrations contribute to the ionic movement. However, their associated elongations are far too small to induce any metallic behavior. At 50 K both the FP and MD configurations remain semiconducting. Though as a result of thermal smearing the conductance is marginally elevated. Increasing the temperature to 300 K, however, reveals a dramatic difference between the conductances predicted by both approaches. The FP approach, assuming stable and well-defined structural phases due to its inherent harmonic approximation, yields a conductance of roughly half than that of a zero temperature calculation for the ideal (4×1) reconstruction. On the other hand, the MD approach predicts an RT conductance that is considerably lower. According to the dynamical fluctuation model, for which MD calculations actually provide the main support, the (4×1) reconstruction is explained as the time-average of a system that is oscillating between the degenerate (8×2) ground states. Since the system frequently visits these semiconducting ground states the conductance is significantly lower than in the case of stable and well-defined structural phases. The conductance obtained from the FP approach overestimates – by roughly a factor of 1.2 – the experimentally determined surface state conductance in the RT regime [37, 39, 40]. This effect is expected due to the neglect of contact resistance. However, the dynamical fluctuation model leads to an underestimation by a factor of 0.76. These results provide a further indication that the dynamical fluctuation model does not describe the physics of the phase transition correctly.

As discussed above, the FP calculations confirm the existence of a low-frequency shear mode of A″ symmetry for the In-Si(111)(4×1) phase at 28 cm^{-1}. This mode, which was also detected by Raman spectroscopy [61], corresponds in conjunction with a twofold degenerate low-frequency X-point mode at 17 cm^{-1} to the lattice deformation characteristic for the $(4 \times 1) \rightarrow (8 \times 2)$ phase transition. According to the dynamical fluctuation model the soft shear mode drives the fluctuations between degenerate ground states. Examining this mode in detail is therefore expected to provide new insights with respect to phase stability. Table 5 lists the frequency of the shear mode obtained by FP and MD calculations in comparison with experimental data from Ref. [61]. Within the MD configurations the shear mode was identified by Fourier-decomposing. Selecting the correct Fourier coefficient and transforming back into the time domain yields very little ionic motion besides the shear mode. The eigenfrequency is then easily obtained from the periodicity of the ionic motion along the FP eigenvector of

Table 4 Average conductances and standard deviations per (8×2) unit cell in linear response obtained for Bose–Einstein occupation of FP modes and from MD calculations.

	frozen-phonon G $[2e^2/h]$	molecular dynamics G $[2e^2/h]$
0 K	0.00 ± 0.00	–
50 K	0.11 ± 0.28	0.22 ± 0.36
300 K	3.09 ± 0.65	1.95 ± 0.86

Table 5 Frequency of the soft shear mode obtained by FP and MD calculations in comparison with experimental data from Ref. [61].

	(8×2) (cm^{-1})	→	(4×1) (cm^{-1})
experiment [61]	$2 \cdot 23.5 \pm 0.8$	→	28 ± 0.9
frozen-phonon	18, 19	→	28
molecular dynamics	20	→	16

the shear mode. However, a clear distinction between the frequencies of the symmetric and antisymmetric shear modes is difficult from the MD data. So only one frequency is given in Table 5. At LTs both approaches agree closely with the measured frequency of the shear mode. Upon the transition to (4 × 1) translational symmetry a blue-shift of the shear mode frequency is observed experimentally. This blue-shift is well reproduced by FP calculations, which implicitly assume that the surface is trapped in the (4 × 1) minimum on the PES. However, according to the dynamical fluctuation model the system was initially trapped in one of the degenerate (8 × 2) minima. Upon heating the surface it begins to fluctuate between the degenerate ground states at activation temperature, thereby giving rise to a (4 × 1) translational symmetry on average. In this case the shear mode would red-shift, rather than blue-shift. Calculating the shear mode's frequency from an MD run at 300 K yields indeed the expected red-shift (*cf.* Table 5), in clear contradiction to experiment.

From the above results it is obvious that the MD simulations, while providing the main support for the dynamic fluctuation model, describe the temperature-dependent vibrational and electron-transport properties of the In-Si(111)(4 × 1)/(8 × 2) nanowire array worse than FP calculations. This result is surprising, given that the harmonic approximation is supposed to introduce noticeable errors in the calculations for elevated temperatures. What is the reason for these discrepancies between experiment and MD simulation? Quantum mechanics requires the occupation of the phonon modes to obey the Bose–Einstein distribution. However, MD employs a Boltzmann distribution over ion velocities instead. Therefore, it is only accurate for sufficiently high temperatures. For the subtle energy balance at the In-Si(111)(4 × 1)/(8 × 2) surface the error at 300 K is still noticeable. The MD simulation at 300 K features an average elongation of the shear mode of 0.43 Å, with a maximum elongation of up to 0.76 Å. This corresponds to excitation energies from 40 meV up to 145 meV, respectively. In contrast, the Bose–Einstein occupation of this mode at 16 cm^{-1} results in an energy expectation value of 26 meV. The overestimation of the occupation of that mode in the MD simulation gives rise to an erroneous observation of dynamical fluctuations.

6 Alkali adsorption perturbs phase transition

Already ten years ago it was noted that tiny amounts of adsorbates, specifically less than 0.1 MLs of Al, Ga, In, or Ag adatoms revert the LT (8 × 2) phase to the (4 × 1) structure usually observed above 120 K [15]. The structural modification was found to be accompanied by an increase in electrical conductivity. This is in contrast to more recent studies [64, 65] which report a decrease of the metal-insulator transition temperature T_C upon In adsorption. Also the exposure of the In nanowires to oxygen was found to increase T_C. Intriguing indirect interactions between the adatoms mediated by the In nanowire CDW were observed for Pb [66] and Co [67] adsorption. Probably most studies in the context of atomic adsorption on the In nanowire array are devoted to the influence of sodium. Using STM, Lee et al. [14] found that the metallic (4 × 1) In zigzag chain structure turns in an insulating system with a doubled periodicity along the chains upon Na deposition. This was attributed to an adsorbate-induced CDW pinning. Density functional calculations by Cho et al. [68], however, found the doubling of the periodicity energetically unfavorable and did not support a Na-induced metal-insulator transition resulting from a CDW gap. In 2008 temperature-dependent low-energy electron diffraction (LEED) data were interpreted in terms of an increase of the transition temperature T_C due to Na adsorption [69], confirming the trend reported in Ref. [14]. In fact, a value of $T_C = 186$ K was reported for the adsorption of 0.1 ML Na. In clear contrast, Shim et al. [70] as well as a very recent study by Yeom and coworkers [71] found an almost linear decrease of T_C with the amount of Na atoms deposited on the In nanowire array. In Ref. [70] a variation between 125 and 90 K is reported for T_C. In Ref. [71] a (4 × 1) LEED pattern was detected at heavily alkali-doped In-Si(111) even at 50 K.

While DFT calculations have contributed greatly to the understanding of the clean nanowire array, we are aware of only relatively few studies addressing computationally the adsorption of adatoms on the nanowires [41, 66, 68, 72]. None of them addresses the influence of adatoms on the (8 × 2)–(4 × 1) phase transition. In the following we perform DFT calculations with the aim to better understand the impact of Na adsorption on the metal-insulator transition of the In-Si(111)(4 × 1)/(8 × 2) surface.

We start by determining the PES for Na adsorbed on the RT (4 × 1) phase of the nanowire array. These calculations are performed in a (4 × 4) unit cell with three bilayers of Si. The calculated energy landscape and the most favored lateral positions for Na adatoms are shown in Fig. 14a. For one Na-adatom per (4 × 4) unit cell we find three nearly degenerate adsorption sites H_1, H_2, and H_3 with adsorption energies of 2.165, 2.150, and 2.174 eV, respectively. At this as well as higher coverages sodium prefers a position between neighboring In and Si chains (H_3). Lowering the coverage to one Na adatom per (8 × 4) unit cell, leads to H_1 being the most stable adsorption site. Our results largely agree with earlier DFT calculations of the Kleinman and coworkers [68] which – using a (4 × 3) unit cell and the generalized gradient approximation – reported adsorption energies of 1.452 and 1.446 eV for adsorption at the H_1 and H_2 site, respectively, while the adsorption between the In and Si zigzag chains was found to be somewhat less favored than in the present work. The corrugation of the PES with a distinct channel along the chain direction suggests a strongly anisotropic diffusion behavior and a high adatom mobility along the In zigzag chains.

The two energetically most relevant structures, H_1 and H_3, are schematically shown in Fig. 15. Obviously Na prefers a pyramidal configuration. The structural deformations of the In nanowire array are comparatively minor. The largest deviation from the ground-state geometry of the clean

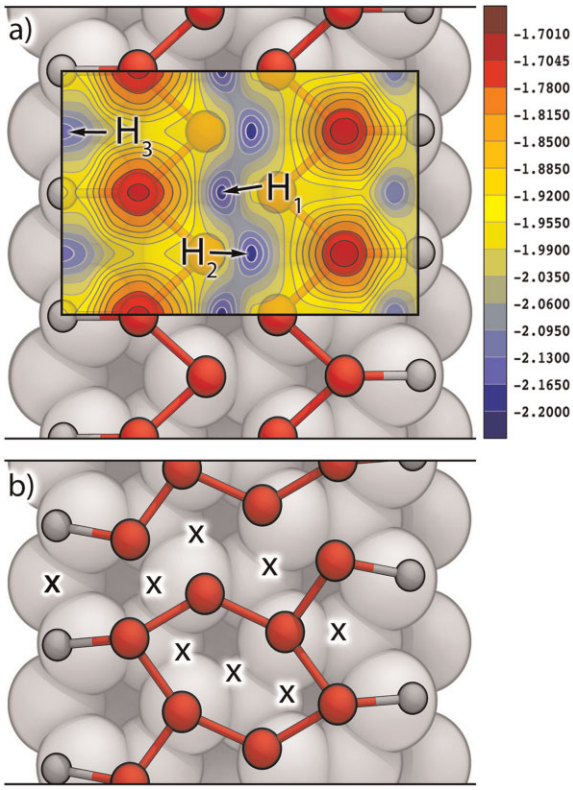

Figure 14 (online color at: www.pss-b.com) (a) PES (in eV) calculated for Na adatoms on the In/Si(111)(4 × 1) surface. Three local minimum energy positions for the adsorbed species are marked. Dark and light balls indicate In and Si positions, respectively. (b) Starting configurations for Na adatoms on the In/Si(111)(8 × 2) surface.

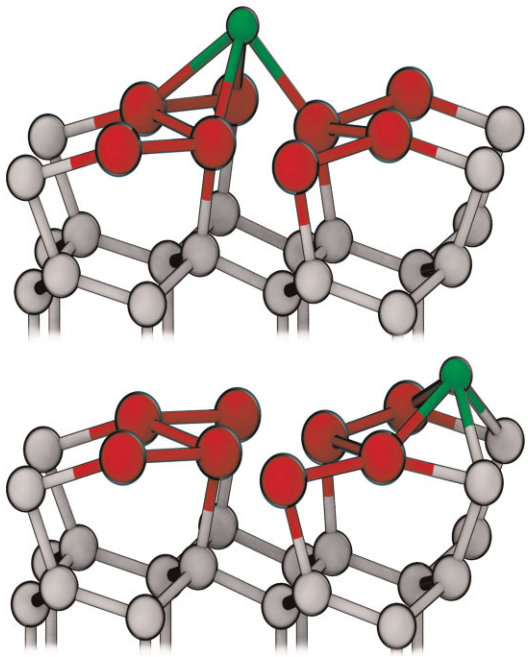

Figure 15 (online color at: www.pss-b.com) Equilibrium structure of Na adsorbed on the In-Si(111)(4 × 1) surface at the H_1 (top) and H_3 (bottom) site.

In-Si(111)(4 × 1) surface occurs in case of the H_1 adsorption and modifies the In–In distance across the two parallel zigzag chains by about 0.16 Å.

In order to probe long-range correlation effects between surface adsorbed adatoms possibly due to adsorbate induced Friedel oscillations [73] we performed calculations for different adatom distances along and perpendicular to the In chains. The results are summarized in Fig. 16. Sodium adsorbed in $H_{1/3}$ position was calculated using a $(4 \times n)$ translational symmetry with $n = 1, 2, 3, 4, 5, 6$. In case of H_1 adsorption it is found that the adsorption energy is monotonously increasing with increasing distance, at least for the distances computationally accessible. In the case of H_3 two rather shallow energy minima are found for $n = 3, 5$. If the adatom distance is increased vertically to the In chains, the energetical order of the two adsorption sites may change: H_1 adsorption is more favored than H_3 adsorption for a (8×4) surface periodicity. While the details of the adsorption geometry will thus depend on the surface coverage as well as the adsorption kinetics, there is a clear overall trend for increased adsorption energy with increased adatom separation. Similar results were obtained in Ref. [68] and explained by an electron transfer from the Na adatoms in the In-chain derived orbitals. Thus, adsorbed Na atoms become effectively positive ions, giving rise to a repulsion interaction. The stability of semiconductor surface reconstructions is often surprisingly well described by the Madelung energy of surface atoms charged according to the electron counting rule, see, *e.g.* [74, 75]. Assuming a similarly simple picture to hold here, we calculated the Coulomb repulsion for a periodic lattice of positively charged Na adatoms, assuming a screening that is approximately given by half the static dielectric constant of Si (due to the reduced screening at the surface). Using the

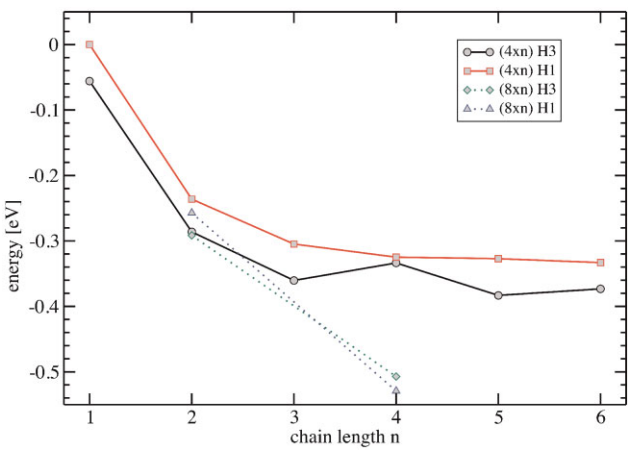

Figure 16 (online color at: www.pss-b.com) Change of the adsorption energy upon increasing the distance between Na adatoms adsorbed for $(4/8 \times n)$ translational symmetry.

charge transfer as fit parameter, it is found that the data of Fig. 15 are well described for a charge transfer of about 0.8*e*. Certainly, the result of such a procedure has to be taken with caution. Nevertheless, it fits well to the ARPES data given in Ref. [71]. Here, it was concluded that roughly a single electron is donated to the surface from each Na adsorbate atom.

The impact of Na adatoms on the In nanowire electronic properties is controversially discussed. There are reports that Na deposition increases [69] as well as decreases [70, 71] the metal-insulator transition temperature T_C. Morikawa et al. [71] performed STM studies and discriminated between two effects of the Na deposition, the global suppression of the metal-insulator transition *versus* a local lattice distortion that results in a reduced DOS at the Fermi energy. While in Ref. [71] it is stated that in spite of the reduced DOS at the Fermi energy the In nanowire remain metallic, the opening of a small gap of about 0.1 eV has been concluded from high-resolution electron-energy-loss spectroscopy (HREELS) data [14].

Before we explore possible implications of the adsorbate atoms on the phase transition, we discuss its local influence on the nanowire electronic properties. Thereby we start from the relaxed adatom positions H_1 as well as H_3 and consider single Na adatoms calculated in a (4 × 8) surface unit cell. According to our DFT calculations, the modification of the DOS is negligible in the intermediate vicinity of the Fermi energy. The metallicity of the nanowires is not affected by the alkali adsorption. However, about 0.1 eV below the Fermi energy a clear reduction in the DOS is calculated for the Na adsystem, both for H_1 and H_3 adsorption. This confirms earlier DFT calculations by the Kleinman and coworkers [68] performed for smaller unit cells, *i.e.*, higher Na coverages. The change of the DOS calculated here for energies below the Fermi may explain HREELS findings for Na-adsorbed nanowires that show the Drude tail due to transitions near the Fermi level to be drastically reduced in width compared to the clean surface [14]. We also studied the influence of the Na adatoms on the In nanowire conductance using the Landauer approach described in Section 3. Compared to the calculations for the ideal structure, a reduction of the quantum conductance at E_F by about one tenth (H_1) to one third (H_3) compared to the ideal chain is obtained for the case of Na adatoms (see Ref. [76] for details). Comparing these data with the results discussed in Section 3 one finds that sodium is about as effective as Pb in hindering the electron transport through the wires. From the calculations we can conclude on a sizeable conductance drop due to the adsorption of Na on the In-Si(111)(4 × 1) surface.

Next, we study the influence of the Na adatoms on the phase transition. At first we adsorbed sodium on the structure of the LT (8 × 2) phase of In-Si(111). Thereby we used the lateral positions indicated in Fig. 14b as starting configurations. Structural relaxation leads to variety of local energy minima. Interestingly, the transformation of the In hexagon structure in the zigzag-chain geometry of the (4 × 1) phase with the Na adatom assuming the H_1 position shown in Fig. 14a represents the global energy minimum among the necessarily limited number of structures investigated. Thus, the alkali adsorption seems to perturb the subtle energy balance between the semiconducting In hexagons and the metallic In zigzag chains in favor of the latter.

The changes in the calculated electronic band structure accompanying the (4 × 1)–(8 × 2) phase transition are shown in Fig. 17. The hexagon formation is related to the opening of a small gap. The charge transfer from the adatoms into the surface lowers the gain in band structure energy upon hexagon formation. This could be one plausible mechanism that explains why Na adsorption tends to favor the formation of the (4 × 1) phase. In order to verify this assumption we follow Ref. [77] and calculate the energy difference between (4 × 1) and (8 × 2) reconstructed In-Si(111) surfaces – in the absence of any alkali adatoms – in dependence on the surface charging. The results are shown in Fig. 18. Obviously, the charging of the surface destabilizes indeed the (8 × 2) surface with respect to the (4 × 1) phase. If one assumes that the adsorption of Na atoms changes the vibrational energy of In-Si(111)(4 × 1) and In-Si(111)(8 × 2) surfaces by a similar amount due to the appearance of new localized phonon modes and neglects any influence of local strain on the phase stability, the change of the phase transition temperature can be estimated from the modification of the difference of the respective total-energies upon charge transfer into the surface calculated above. We thus obtain the phase transition temperatures indicated on the right hand side in Fig. 18. From the data shown in Fig. 17 we would thus predict a phase transition temperature of $T_C = 97$ K for a Na coverage of 0.01 ML. Given that – as argued above – the local strain induced by the Na adsorption also favors In zigag chains rather hexagons, this temperature should be considered an upper

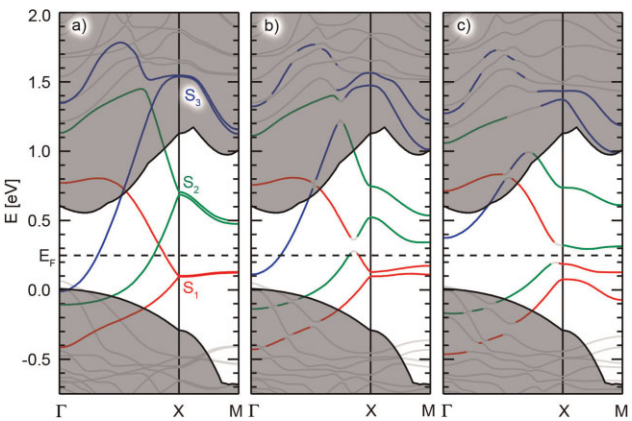

Figure 17 (online color at: www.pss-b.com) Band structures of the zigzag chain (a) and hexagon model (c) of the In-Si(111) surface calculated within a (4 × 2) surface unit cell. The electron bands of a transitional structure obtained from the superposition of the phonon modes that transform between these structural models (see Ref. [25]) is shown in (b). Bands of equal color are characterized by similar wave functions.

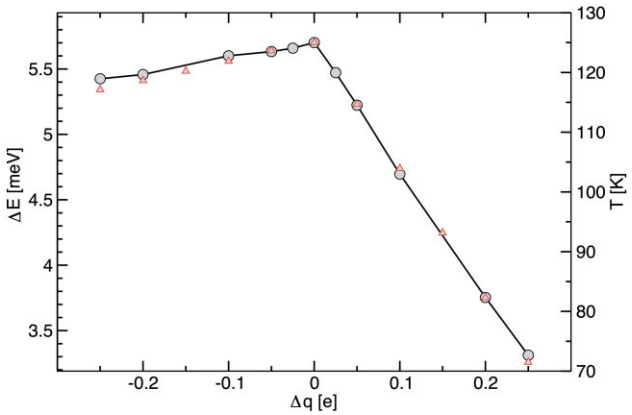

Figure 18 (online color at: www.pss-b.com) Difference in total energy (per surface atom) between In-Si(111)(4×1) and In-Si(111)(8×2) surfaces in dependence on the surface charging (per (8×2) surface unit cell). The right scale indicates the phase transition temperature predicted for the respective charging assuming that the adatoms modify the vibrational entropy of (4×1) and (8×2) surfaces by the same amount. Circles and triangles indicate energies obtained with and without structural relaxation, respectively.

limit for the actual value. Unfortunately, the present experimental findings do not allow for a direct comparison, as no detailed information on the coverage dependent value of T_C is available. The order of magnitude predicted here, however, seems to agree with the recent experimental data reported in Refs. [70, 71].

On the other hand, Na deposition at very LTs will not necessarily lead to the ground-state geometry where local strains favors the zigzag chain formation. It is very well conceivable that Na adsorption at some metastable position leads to geometrical constraints that favor hexagons and thus lead to an apparent pinning of the In-Si(111)(8×2) surface.

From Fig. 18 it is clear that a reduction of the phase transition temperature should also occur in case of *p*-doping. This appears plausible in the picture discussed above, because the energetic preference of the insulating (8×2) reconstructed In-Si(111) surface over the metallic (4×1) will be reduced no matter in which direction the Fermi energy is shifted. However, we are not aware of an experimental study in this context.

7 Summary This paper summarized briefly the recent progress in the understanding of the structural and electron transport properties of the prototypical In-Si(111)(4×1)/(8×2) nanowire array. The RT (4×1) reconstructed In-Si(111) surface is characterized by In zigzag chains giving rise to three pronounced surface states at the Fermi energy. The dispersion of these surfaces explains naturally the strong anisotropy of the electron conductance along and perpendicular to the chain direction. There is no need to assume contributions from the space charge layer in order to reproduce the experimental results. The adsorption of adatoms is predicted to lead to a specific and in some cases pronounced decrease of the wire conductivity. For In adatoms, where measurements exist, the calculated reduction by more than one third agrees with the existing data. For oxygen deposition, the calculations predict a similar drop in conductance, whereas the impact of Pb and Na atoms is slightly smaller. The reduction of the nanowire conductance can be traced to either potential-well scattering or the quenching of conduction channels due to nanowire deformation or a combination of both effects. According to the DFT calculations, the adsorption of hydrogen does not substantially reduce the conductance.

While previous experiments as well as total-energy calculations have not been able to unambiguously identify the geometry of the (8×2) reconstructed In-Si(111) surface formed at LTs, the comparison of the calculated spectral signatures with the experimental data gives strong evidence for the formation of In hexagons. In particular, strong anisotropic optical interband transitions are found at 0.50 and 0.72 eV for the In-Si(111)(8×2) phase. In contrast to the trimer model, optical response calculations for the hexagon model reproduced the measured features. In particular, the 0.7 eV peak arises from optical transitions involving the additional In–In bonds that are formed in the hexagon model. These results settle the long-standing argument about the In nanowire ground state in favor of the hexagon model.

Free energy calculations explain the (4×1)–(8×2) phase transition of the In-Si(111) nanowire array in terms of a subtle interplay between the lower total energy of the insulating In hexagon structure and the larger vibrational and electronic entropy of the less tightly bound and metallic In zigzag chain structure at finite temperatures. Both the (4×1) and (8×2) phases are stable and well-defined structural phases. Soft shear and rotary vibrations transform between the In zigzag chains stable at RT and the hexagons formed at LTs. The present work resolves the discrepancies arising from the interpretation of the (4×1) reconstruction as time-averaged superposition of (8×2) structures given by the dynamic fluctuation model. In fact, we could show that the order–disorder model for the phase transition does not account for the measured electron transport properties and phonon frequencies shifts. MD calculations that provide the main support for a order–disorder type phase transition do not describe the surface dynamics entirely correct, due to the classical velocity distribution employed.

Sodium adsorption on the In nanowire array has a strong influence on its phase change. The present calculations show that the LT (8×2) phase gets destabilized due to the charge transfer from the adatoms into the In nanowires as well as due to local strain. This leads to a decrease of the phase-transition temperature and may trigger an insulator-metal transition at specific temperatures.

Acknowledgements We have benefited from discussions with many colleagues on the subject matter. In particular we acknowledge detailed discussions with F. Bechstedt, N. Esser,

K. Fleischer, F. Flores, J. Ortega, E. Speiser, A. A. Stekolnikov, and H. W. Yeom. We gratefully acknowledge financial support from the Deutsche Forschungsgemeinschaft as well as supercomputer time provided by the HLRS Stuttgart and the Paderborn PC^2.

References

[1] F. J. Himpsel, K. N. Altman, R. Bennewitz, J. N. Crain, A. Kirakosian, J. L. Lin, and J. L. McChesney, J. Phys.: Condens. Matter **13**, 11097 (2001).
[2] C. Blumenstein, J. Schäfer, S. Mietke, S. Meyer, A. Dollinger, M. Lochner, X. Y. Cui, L. Patthey, R. Matzdorf, and R. Claessen, Nature Phys. **7**(8), 1 (2011).
[3] J. J. Lander and J. Morrison, J. Appl. Phys. **36**, 1706 (1965).
[4] O. Bunk, G. Falkenberg, J. H. Zeysing, L. Lottermoser, R. L. Johnson, M. Nielsen, F. Berg-Rasmussen, J. Baker, and R. Feidenhans'l, Phys. Rev. B **59**, 12228 (1999).
[5] J. H. Cho, D. H. Oh, K. S. Kim, and L. Kleinman, Phys. Rev. B **64**, 235302 (2001).
[6] J. Nakamura, S. Watanabe, and M. Aono, Phys. Rev. B **63**, 193307 (2001).
[7] R. H. Miwa and G. P. Srivastava, Surf. Sci. **473**, 123 (2001).
[8] S. Wang, W. Lu, W. G. Schmidt, and J. Bernholc, Phys. Rev. B **68**, 035329 (2003).
[9] K. Fleischer, S. Chandola, N. Esser, W. Richter, and J. F. McGilp, Phys. Rev. B **67**, 235318 (2003).
[10] J. H. Cho, J. Y. Lee, and L. Kleinman, Phys. Rev. B **71**, 081310(R) (2005).
[11] S. F. Tsay, Phys. Rev. B **71**, 035207 (2005).
[12] X. Lopez-Lozano, A. Krivosheeva, A. A. Stekolnikov, L. Meza-Montes, C. Noguez, J. Furthmüller, and F. Bechstedt, Phys. Rev. B **73**, 035430 (2006).
[13] G. Lee, S. Y. Yu, H. Kim, and J. Y. Koo, Phys. Rev. B **70**, 121304(R) (2004).
[14] S. S. Lee, J. R. Ahn, N. D. Kim, J. H. Min, C. G. Hwang, J. W. Chung, H. W. Yeom, S. V. Ryjkov, and S. Hasegawa, Phys. Rev. Lett. **88**, 196401 (2002).
[15] S. V. Ryjkov, T. Nagao, V. G. Lifshits, and S. Hasegawa, Surf. Sci. **488**, 15 (2001).
[16] H. W. Yeom, S. Takeda, E. Rotenberg, I. Matsuda, K. Horikoshi, J. Schaefer, C. M. Lee, S. D. Kevan, T. Ohta, T. Nagao, and S. Hasegawa, Phys. Rev. Lett. **82**, 4898 (1999).
[17] C. Gonzalez, J. Ortega, and F. Flores, New J. Phys. **7**, 100 (2005).
[18] S. J. Park, H. W. Yeom, J. R. Ahn, and I. W. Lyo, Phys. Rev. Lett. **95**, 126102 (2005).
[19] J. Guo, G. Lee, and E. W. Plummer, Phys. Rev. Lett. **95**, 046102 (2005).
[20] C. Gonzalez, F. Flores, and J. Ortega, Phys. Rev. Lett. **96**, 136101 (2006).
[21] A. A. Stekolnikov, K. Seino, F. Bechstedt, S. Wippermann, W. G. Schmidt, A. Calzolari, and M. Buongiorno Nardelli, Phys. Rev. Lett. **98**, 026105 (2007).
[22] U. Häussermann, S. I. Simak, R. Ahuja, B. Johansson, and S. Lidin, Angew. Chem., Int. Ed. **38**, 2017 (1999).
[23] S. I. Simak, U. Häussermann, R. Ahuja, S. Lidin, and B. Johansson, Phys. Rev. Lett. **85**, 142 (2000).
[24] S. Chandola, K. Hinrichs, M. Gensch, N. Esser, S. Wippermann, W. G. Schmidt, F. Bechstedt, K. Fleischer, and J. F. McGilp, Phys. Rev. Lett. **102**(22), 226805 (2009).
[25] S. Wippermann and W. G. Schmidt, Phys. Rev. Lett. **105**, 126102 (2010).
[26] D. M. Ceperley and B. J. Alder, Phys. Rev. Lett. **45**, 566 (1980).
[27] G. Kresse and J. Furthmüller, Comput. Mater. Sci. **6**, 15 (1996).
[28] A. Calzolari, N. Marzari, I. Souza, and M. B. Nardelli, Phys. Rev. B **69**, 035108 (2004).
[29] Y. S. Lee, M. B. Nardelli, and N. Marzari, Phys. Rev. Lett. **95**, 076804 (2005).
[30] S. Riikonen, A. Ayuela, and D. Sanchez-Portal, Surf. Sci. **600**, 3821 (2006).
[31] S. Wippermann, W. G. Schmidt, A. Calzolari, M. B. Nardelli, A. A. Stekolnikov, K. Seino, and F. Bechstedt, Surf. Sci. **601**, 4045 (2007).
[32] J. McGilp, Prog. Surf. Sci. **49**(1), 1 (1995).
[33] R. Del Sole, Solid State Commun. **37**, 537 (1981).
[34] W. G. Schmidt, Phys. Status Solidi B **242**, 2751 (2005).
[35] P. H. Hahn, W. G. Schmidt, and F. Bechstedt, Phys. Rev. Lett. **88**, 016402 (2001).
[36] W. G. Schmidt, S. Glutsch, P. H. Hahn, and F. Bechstedt, Phys. Rev. B **67**, 085307 (2003).
[37] T. Kanagawa, R. Hobara, I. Matsuda, T. Tanikawa, A. Natori, and S. Hasegawa, Phys. Rev. Lett. **91**, 036805 (2003).
[38] R. S. Sorbello, Phys. Status Solidi B **107**(1), 233 (1981).
[39] T. Tanikawa, I. Matsuda, T. Kanagawa, and S. Hasegawa, Phys. Rev. Lett. **93**, 016801 (2004).
[40] T. Uchihashi and U. Ramsperger, Appl. Phys. Lett. **80**, 4169 (2002).
[41] S. Wippermann, N. Koch, and W. G. Schmidt, Phys. Rev. Lett. **100**, 106802 (2008).
[42] A. Calzolari, C. Cavazzoni, and M. B. Nardelli, Phys. Rev. Lett. **93**, 096404 (2004).
[43] K. Sakamoto, H. Ashima, H. W. Yeom, and W. Uchida, Phys. Rev. B **62**, 9923 (2000).
[44] H. W. Yeom, K. Horikoshi, H. M. Zhang, K. Ono, and R. I. G. Uhrberg, Phys. Rev. B **65**, 241307(R) (2002).
[45] S. J. Park, H. W. Yeom, S. H. Min, D. H. Park, and I. W. Lyo, Phys. Rev. Lett. **93**, 106402 (2004).
[46] Y. J. Sun, S. Agario, S. Souma, K. Sugawara, Y. Tago, T. Sato, and T. Takahashi, Phys. Rev. B **77**(12), 125115 (2008).
[47] J. R. Ahn, J. H. Byun, H. Koh, E. Rotenberg, S. D. Kevan, and H. W. Yeom, Phys. Rev. Lett. **93**(10), 106401 (2004).
[48] J. H. Cho and J. Y. Lee, Phys. Rev. B **76**(3), 033405 (2007).
[49] Y. Fukaya, M. Hashimoto, A. Kawasuso, and A. Ichimiya, Surf. Sci. **602**(14), 2448–22452 (2008).
[50] F. Pedreschi, J. D. O'Mahony, P. Weightman, and J. R. Power, Appl. Phys. Lett. **73**, 2152 (1998).
[51] J. F. McGilp, Phys. Status Solidi A **188**, 1361 (2001).
[52] K. Fleischer, S. Chandola, N. Esser, W. Richter, and J. F. McGilp, Phys. Status Solidi A **188**, 1411 (2001).
[53] K. Fleischer, S. Chandola, N. Esser, W. Richter, J. F. Mcgilp, W. G. Schmidt, S. Wang, W. Lu, and J. Bernholc, Appl. Surf. Sci. **234**(1–4), 302–306 (2004).
[54] S. Wippermann and W. G. Schmidt, Surf. Sci. **603**, 247 (2009).
[55] S. Wippermann, Understanding substrate-supported atomic-scale nanowires from ab initio theory, PhD thesis, Universität Paderborn, Paderborn, 2010.
[56] T. Abukawa, M. Sasaki, F. Hisamatsu, T. Goto, T. Kinoshita, A. Kakizaki, and S. Kono, Surf. Sci. **325**, 33 (1995).
[57] J. R. Ahn, J. H. Byun, H. Koh, E. Rotenberg, S. D. Kevan, and H. W. Yeom, Phys. Rev. Lett. **93**, 106401 (2004).

[58] C. Kumpf, O. Bunk, J. H. Zeysing, Y. Su, M. Nielsen, R. L. Johnson, R. Feidenhans'l, and K. Bechgaard, Phys. Rev. Lett. **85**, 4916 (2000).
[59] C. González, J. Guo, J. Ortega, F. Flores, and H. H. Weitering, Phys. Rev. Lett. **102**(11), 115501 (2009).
[60] H. W. Yeom, Phys. Rev. Lett. **97**(18), 189701 (2006).
[61] K. Fleischer, S. Chandola, N. Esser, W. Richter, and J. F. McGilp, Phys. Rev. B **76**, 205406 (2007).
[62] M. Valtiner, M. Todorova, G. Grundmeier, and J. Neugebauer, Phys. Rev. Lett. **103**(6), 065502 (2009).
[63] F. Bechstedt, A. Krivosheeva, J. Furthmüller, and A. A. Stekolnikov, Phys. Rev. B **68**, 193406 (2003).
[64] W. Lee, H. Shim, and G. Lee, J. Korean Phys. Soc. **56**, 943 (2010).
[65] T. Shibasaki, N. Nagamura, T. Hirahara, H. Okino, S. Yamazaki, W. Lee, H. Shim, R. Hobara, I. Matsuda, G. Lee, and S. Hasegawa, Phys. Rev. B **81**(3), 035314 (2010).
[66] M. Hupalo, T. L. Chan, C. Z. Wang, K. M. Ho, and M. C. Tringides, Phys. Rev. B **76**, 045415 (2007).
[67] C. Liu, T. Uchihashi, and T. Nakayama, Phys. Rev. Lett. **101**, 146104 (2008).
[68] J. H. Cho, D. H. Oh, and L. Kleinman, Phys. Rev. B **66**, 075423 (2002).
[69] S. S. Lee, S. Y. Shin, C. G. Hwang, and J. W. Chung, J. Korean Phys. Soc. **53**, 3667 (2008).
[70] H. Shim, S. Y. Yu, W. Lee, J. Y. Koo, and G. Lee, Appl. Phys. Lett. **94**(23), 231901 (2009).
[71] H. Morikawa, C. C. Hwang, and H. W. Yeom, Phys. Rev. B **81**(7), 075401 (2010).
[72] S. Y. Yu, D. Lee, H. Kim, J. Y. Koo, and G. Lee, J. Korean Phys. Soc. **48**, 1338, (2006).
[73] S. Blankenburg and W. G. Schmidt, Phys. Rev. B **78**, 233411 (2008).
[74] W. G. Schmidt, Appl. Phys. A **65**, 581 (1997).
[75] W. G. Schmidt, Appl. Phys. A **75**, 89 (2002).
[76] W. G. Schmidt, M. Babilon, C. Thierfelder, S. Sanna, and S. Wippermann, Phys. Rev. B **84**, 115416 (2011).
[77] K. Seino, W. G. Schmidt, and F. Bechstedt, Phys. Rev. Lett. **93**, 036101 (2004).